

A Nonlinear Dynamics-Based Estimator for Functional Electrical Stimulation: Preliminary Results From Lower-Leg Extension Experiments

Marcus Allen, Qiang Zhong, Nicholas Kirsch, Ashwin Dani, *Member, IEEE*, William W. Clark, and Nitin Sharma

Abstract—Miniature inertial measurement units (IMUs) are wearable sensors that measure limb segment or joint angles during dynamic movements. However, IMUs are generally prone to drift, external magnetic interference, and measurement noise. This paper presents a new class of nonlinear state estimation technique called state-dependent coefficient (SDC) estimation to accurately predict joint angles from IMU measurements. The SDC estimation method uses limb dynamics, instead of limb kinematics, to estimate the limb state. Importantly, the nonlinear limb dynamic model is formulated into state-dependent matrices that facilitate the estimator design without performing a Jacobian linearization. The estimation method is experimentally demonstrated to predict knee joint angle measurements during functional electrical stimulation of the quadriceps muscle. The nonlinear knee musculoskeletal model was identified through a series of experiments. The SDC estimator was then compared with an extended kalman filter (EKF), which uses a Jacobian linearization and a rotation matrix method, which uses a kinematic model instead of the dynamic model. Each estimator's performance was evaluated against the true value of the joint angle, which was measured through a rotary encoder. The experimental results showed that the SDC estimator, the rotation matrix method, and EKF had root mean square errors of 2.70° , 2.86° , and 4.42° , respectively. Our preliminary experimental results show the new estimator's advantage over the EKF method but a slight advantage over the rotation matrix method. However, the information from the dynamic model allows the SDC method to use only one IMU to measure the knee angle compared with the rotation matrix method that uses two IMUs to estimate the angle.

Index Terms—State-dependent coefficient, extended kalman filter, rotation matrix, functional electrical stimulation, nonlinear state estimator.

Manuscript received September 23, 2016; revised April 15, 2017; accepted August 20, 2017. Date of publication September 7, 2017; date of current version November 29, 2017. This work was supported by the NSF under Award 1462876 and Award 1511139 and in part by the NIH under Grant R03HD086529-01. (Corresponding author: Nitin Sharma.)

M. Allen, Q. Zhong, N. Kirsch, and W. W. Clark are with the Department of Mechanical Engineering and Materials Science, University of Pittsburgh, Pittsburgh, PA 15260 USA (e-mail: mca36@pitt.edu; qiangzhong@pitt.edu; nak65@pitt.edu; wclark@pitt.edu).

A. Dani is with the Department of Electrical Engineering, University of Connecticut, Storrs, CT 06269 USA (e-mail: ashwin.dani@uconn.edu).

N. Sharma is with the Department of Mechanical Engineering and Materials Science, University of Pittsburgh, Pittsburgh, PA 15260 USA, and also with the Department of Bioengineering, University of Pittsburgh, Pittsburgh, PA 15260 USA (e-mail: nis62@pitt.edu).

Digital Object Identifier 10.1109/TNSRE.2017.2748420

I. INTRODUCTION

FUNCTIONAL electrical stimulation (FES) is used to restore limb functions in persons with neurological disorders such as spinal cord injury (SCI), multiple sclerosis, and stroke. It generates motion by applying low-level repetitive external electrical currents to peripheral motor neurons. FES systems have been shown to restore reach and grasp function [1], [2], sit-to-stance function [3], drop foot correction [4], and gait restoration [5].

While closed-loop control design for FES has received increased attention, design of high performance estimation methods that predict limb state has been a neglected research topic in FES. Research in the latter is needed if the sensor measurements are noisy and prone to disturbances. For example, accurate measurements are critical in an FES application that corrects drop foot [6]. Inaccurate angle measurements may lead to nerve stimulation at wrong times, potentially destabilizing the swing phase, which may lead to a fall.

Another major motivation to design limb angle estimation algorithms is to develop a wearable means of gait measurement. Optical motion analysis systems are designed for indoor use and cannot be used outside the laboratory environment. Optical encoders, which are often installed in exoskeletal rigid mechanical attachments, are reliable and accurate sensors for limb angle measurement (see [7], [8]). However, these sensors are not suitable for a wearable FES device. A wearable method of measurement uses inertial measurement units (IMUs) that consist of three gyroscopes, accelerometers, and magnetometers [9]–[11]. Many wearable FES systems developed for the correction of drop foot use a single IMU to measure shank angle [4], [9], [12], [13]. This is primarily to replace foot switches, which are unreliable and require wearing shoes. Also, accelerometers and gyroscopes provide a more reliable alternative solution to goniometers which need to be calibrated after every use as goniometers are prone to slippage. IMUs are reliable sensors and do not require calibration. However, they are prone to measurement noise, drift, and external interference [4], [9], [12]–[14], and hence without a filtering algorithm IMUs can severely deteriorate estimation accuracy.

Accurate joint angle estimation may be achieved through model constraint methods [15]–[17], fusion of inertial and

magnetic sensing [18], [19], and multi-sensor fusion using cameras, GPS, and laser range finders (see [20] and references therein). However, model constraint methods are not resistant to erroneous measurements and additional sensors such as laser range finders and cameras add bulk to the system. Limb angle estimation algorithms have employed a Kalman filter [9], [19], [21], a complementary filter that uses acceleration measurements as correction signals [6], [22], an extended Kalman filter [15], [16], [18], [23], [24], unscented Kalman filter [17], and a resetting algorithm to correct drift in a gyroscope [10], [14]. However, these studies either use only limb kinematics (i.e., the underlying musculoskeletal dynamics is neglected) or linearize the measurement model. A kinematics-based measurement model does not capture inertial effects and may not estimate as accurately as a dynamics-based estimation. The EKF algorithm that uses a Jacobian linearization at each previous estimate may introduce large errors during estimation, especially when the measurement model is highly nonlinear.

Recently, a new class of nonlinear estimators, called a state dependent coefficient (SDC) estimator, was suggested for limb angle measurement during FES-elicited tasks [25], [26]. The new estimator avoids Jacobian linearization of nonlinear dynamics. The dynamic model-based method uses known FES inputs, the musculoskeletal dynamics instead of a kinematic model, and estimates of noise and process covariances to estimate limb joint angles. Simulations have shown that the SDC estimator can improve the joint estimation performance compared to an EKF estimator. The estimators were simulated on a three link dynamic gait model [27]. The method's theoretical development, stability, and its convergence for stochastic nonlinear systems is given in [28] and [29].

The main contribution of this paper is that a dynamics-based estimation approach is used to estimate the limb state instead of using a kinematics-based measurement model. It is a first preliminary demonstration of the SDC estimator during FES-elicited tasks. Unlike EKF, which uses Jacobian linearization, an extended linearization is used to alternatively formulate the nonlinear dynamics into SDC parameterized matrices for the estimation process. These multiple SDC parameterizations can be, potentially, optimally weighted and thus, an optimally weighted multiple estimation filter design can be accomplished for a nonlinear estimation problem. In this paper the model-specific SDC-based parameterizations were derived for FES-driven nonlinear musculoskeletal dynamics. The estimator was experimentally validated by obtaining an accurate estimate of the knee joint angle during FES of the quadriceps muscle. The subject-specific parameters for the knee extension dynamic model during FES were experimentally identified for both legs of three able-bodied subjects. The SDC estimator was compared with two different IMU based estimation techniques: a rotation matrix method and an EKF method. A rotation matrix procedure, modified from [30], that related the orientation of the two IMUs in a shared frame of reference was used to obtain the knee joint angle. The EKF method used the Jacobian linearization of the musculoskeletal dynamics for state estimation during FES. The estimators were compared using kinematic data collected during multiple

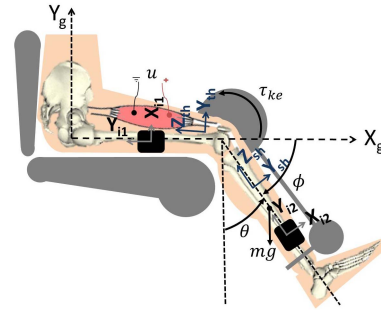


Fig. 1. Leg extension musculoskeletal model. Five coordinate systems are displayed where subscripts: i, th, sh and g represent the IMU, thigh, shank and global frames respectively.

experimental trials that were performed on the both legs of the three able-bodied subjects.

II. SYSTEM DYNAMICS

The dynamics of a leg extension musculoskeletal system during FES, as shown in Fig. 1, is given by

$$J\ddot{\theta} + G(\theta) = \tau_p + \tau_{ke}, \quad (1)$$

where $J \in \mathbb{R}^+$ denotes the moment of inertia of the lower leg, $\theta, \dot{\theta}, \ddot{\theta} \in \mathbb{R}$ are the angular position, velocity, and acceleration of the lower leg, $G(\theta) = mgl_c \sin(\theta)$ is the gravitational torque where $m \in \mathbb{R}^+$ is the mass of lower leg, $g \in \mathbb{R}^+$ is gravitational acceleration, $l_c \in \mathbb{R}^+$ is the length from the mass center of the lower leg to knee joint, and $\tau_p \in \mathbb{R}$ represents the passive musculoskeletal torque of the knee joint, which is modeled as

$$\tau_p = d_1(\phi - \phi_0) + d_2\dot{\phi} + d_3e^{d_4\phi} - d_5e^{d_6\phi}, \quad (2)$$

where $d_i \in \mathbb{R}$, $i = 1, 2, \dots, 6$ and $\phi_0 \in \mathbb{R}$ are subject specific parameters that model the stiffness and damping of the knee joint. In this paper, $\phi, \dot{\phi} \in \mathbb{R}$ represent the anatomical knee joint angle and angular velocity, respectively that are defined as $\phi = \frac{\pi}{2} - \theta$ and $\dot{\phi} = -\dot{\theta}$. In Eq. (1), $\tau_{ke} \in \mathbb{R}$ is the torque produced by muscle contraction and is modeled as

$$\tau_{ke} = (c_2\phi^2 + c_1\phi + c_0)(1 + c_3\dot{\phi})a_{ke}, \quad (3)$$

where $c_i \in \mathbb{R}$, $i = 0, 1, 2, 3$ represent the force-length parameters of the dynamic model. The muscle activation variable $a_{ke} \in \mathbb{R}$ is modeled as a first order system as shown below

$$\dot{a}_{ke} = \frac{u - a_{ke}}{T_a}, \quad (4)$$

where $u \in [0, 1]$ is the normalized electrical stimulation amplitude and $T_a \in \mathbb{R}^+$ is the time constant of muscle activation. The normalized electrical stimulation amplitude can be mapped to the current amplitude of the electrical stimulation as

$$I = I_t + u(I_s - I_t), \quad (5)$$

in which $I_t, I_s \in \mathbb{R}^+$ represent the minimum current amplitude required to produce a movement (threshold) and the minimum current amplitude that produces the maximum muscle force (saturation), respectively. The dynamic system

in Eq. (1)- Eq. (4) can be expressed in state space form as follows

$$\dot{x} = f(x, u) + \omega, \quad (6)$$

where

$$f(x, u) = \begin{bmatrix} x_2 \\ -\beta \sin(x_1) + \alpha(\tau_p + \tau_{ke}) \\ -a_{ke}/T_a + u/T_a \end{bmatrix},$$

$x = [x_1 \ x_2 \ x_3]^T = [\theta \ \dot{\theta} \ a_{ke}]^T$ with $\alpha = 1/J$, $\beta = mgl_c\alpha$ and $\omega = [0 \ \omega_2 \ \omega_3/T_a]^T$ is process noise characterized by Gaussian process and associated with the process noise covariance matrix $Q \in \mathbb{R}^{3 \times 3}$. The measurement model is shown as follows

$$\begin{aligned} y &= h(x) + v = [h_1 \ h_2]^T + v, \\ h_1 &= x_2 - B_{gyro}, \\ h_2 &= -g \sin(x_1), \end{aligned} \quad (7)$$

where h_1 denotes the angular velocity around Z-axis of shank body frame (Z_{sh}), B_{gyro} represents the gyroscope bias, h_2 denotes the acceleration measurement in the Y-axis of the shank body frame (Y_{sh}), and $v \in \mathbb{R}^2$ is a zero-mean Gaussian measurement noise with the measurement covariance matrix $S \in \mathbb{R}^{2 \times 2}$. The gyroscope bias was calculated by taking the average of the signal during the stationary portion of the test. The angular acceleration is ignored in the measurement model. Therefore the acceleration measurement on Y_{sh} can be assumed as pure gravitational acceleration projection on this axis.

III. STATE ESTIMATION

In this section, three state estimation techniques are presented: 1) dynamics-based new nonlinear SDC estimation technique, 2) dynamics-based Extended Kalman Filter method, and 3) kinematics-based Rotation Matrix method. A block diagram of each method is provided in Fig. 2.

A. Nonlinear SDC Estimation and SDC Parameterization

The SDC estimator is based on the dynamic model given in Eq. (6) and the measurement model in Eq. (7). Unlike the EKF, which uses Jacobian computed at a previous state estimate, the SDC estimator implements an extended linearization form or SDC form. The advantage of the SDC form is that the optimal gain of the nonlinear estimator is computed using multiple SDC matrices based uncertainty minimization criteria [25]. The nonlinear dynamics in Eq. (6) can be written into the SDC form as

$$\dot{x} = A_i(x)x + B + w, \quad \forall i = \{1..n\} \quad (8)$$

where $A_i(x)x + B = f(x, u)$. Because SDC parameterizations of the dynamics in Eq. (6) are not unique and different SDC parameterization forms can cause estimation results to vary, a convex combination of $A_i(x) \in \mathbb{R}^{3 \times 3}$ matrices were used to increase the accuracy of the estimation. The convex combination is given as

$$A(x)x = \rho_1 A_1(x)x + \dots + \rho_n A_n(x)x, \quad (9)$$

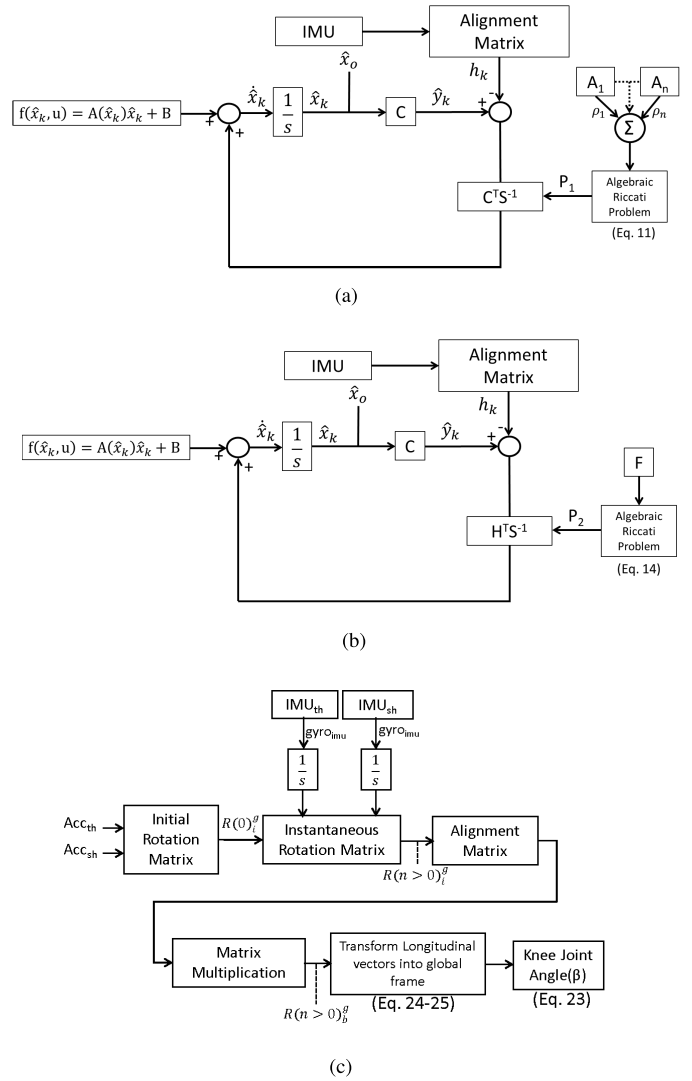


Fig. 2. (a) The block diagram of the SDC estimator method using n SDC parameterizations. The number of parameterizations can be increased as per a user's choice. In the paper, 4 SDC parameterizations were used. The k subscript represents time. (b) The block diagram of the EKF estimator method. (c) The block diagram of the Rotation Matrix method.

where $\rho_1, \dots, \rho_n \geq 0$ and $\sum_{i=1}^n \rho_i = 1$, and ρ_i represents the weights assigned to each SDC parameter. The matrices $A_i(x)$ for ($i = 1$ to 4) are given in Appendix.

In Eq. (8), $B \in \mathbb{R}^3$ is defined as

$$B \triangleq \begin{bmatrix} 0 & \tau_{pre} & u/T_a \end{bmatrix}^T,$$

where

$$\tau_{pre} = d_3 e^{d_4 \frac{\pi}{2}} - d_5 e^{d_6 \frac{\pi}{2}} + d_1 \left(\frac{\pi}{2} - \phi_0 \right).$$

The measurement model in Eq. (7) can be parameterized as

$$y = C(x)x + v,$$

where the output matrix $C(x) \in \mathbb{R}^{2 \times 3}$ is defined as

$$C(x) \triangleq \begin{bmatrix} 0 & 1 & 0 \\ -g \sin(x_1)/x_1 & 0 & 0 \end{bmatrix}.$$

The $A_i(\hat{x})$ and $C(\hat{x})$ were selected so that the pair $A_i(\hat{x}), C(\hat{x})$ is uniformly observable. The SDC based filter is given by

$$\begin{aligned}\dot{\hat{x}} &= f(\hat{x}, u) + K_1(\hat{x}, t)(y - h(\hat{x})), \\ K_1(\hat{x}, t) &= P_1(t)C^T(\hat{x})S^{-1},\end{aligned}\quad (10)$$

where $P_1(t) \in \mathbb{R}^{3 \times 3}$ represents the propagated error covariance matrix and is obtained by solving the algebraic Riccati equation

$$\begin{aligned}A(\hat{x})P_1 + P_1A^T(\hat{x}) + 2aP_1 \\ - 2P_1(C^T(\hat{x})S^{-1}C(\hat{x}))P_1 + LQL^T = 0,\end{aligned}\quad (11)$$

in this case, we chose $a = 0.5$. The Jacobian matrix $L \in \mathbb{R}^{3 \times 3}$ in Eq. (11) is defined as

$$L \triangleq \left. \frac{\partial f(x, u)}{\partial w} \right|_{\hat{x}} = \begin{bmatrix} 0 & 0 & 0 \\ 0 & 1 & 0 \\ 0 & 0 & \frac{1}{T_a} \end{bmatrix}.\quad (12)$$

The zero-mean Gaussian process noise and measurement noise covariance matrices, $Q \in \mathbb{R}^{3 \times 3}$ and $S \in \mathbb{R}^{2 \times 2}$, are given by

$$Q = \begin{bmatrix} q_1 & 0 & 0 \\ 0 & q_2 & 0 \\ 0 & 0 & q_3 \end{bmatrix}, \quad S = \begin{bmatrix} s_1 & 0 \\ 0 & s_2 \end{bmatrix},$$

the process and measurement noise matrices Q and S are constant matrices with a diagonal structure, where the $q_1, q_2, q_3 \in \mathbb{R}$ and $s_1, s_2 \in \mathbb{R}$ were determined by tuning for best performance. The parameters used for both estimators is shown in Appendix. Once \hat{x} was obtained using Eq. (10), the next state was obtained using the fourth order formula of the Runge-Kutta numerical integration method.

B. Extended Kalman Filter

A continuous Extended Kalman Filter (EKF) was proposed to compare the performance of SDC estimator. The EKF algorithm computes, \hat{x} , as follows

$$\begin{aligned}\dot{\hat{x}} &= f(\hat{x}, u) + K_2(t)(y - h(\hat{x})), \\ K_2(t) &= P_2(t)H^T(t)S^{-1},\end{aligned}\quad (13)$$

where $H(x(t)) \in \mathbb{R}^{2 \times 3}$, defined as $H(t) = \left. \frac{\partial h(x)}{\partial x} \right|_{\hat{x}}$ are the linearized measurement model matrix. The error covariance matrix $P_2(t)$ in Eq. (13) was obtained by integrating the following equation

$$\dot{P}_2 = FP_2(t) + P_2F^T - P_2H^T S^{-1}H(t)P_2 + LQL^T \quad (14)$$

where L is defined in Eq. (12) and $F(x(t)) \in \mathbb{R}^{3 \times 1}$, defined as $F(t) = \left. \frac{\partial f(\hat{x}, u)}{\partial x} \right|_{\hat{x}}$.

C. Kinematics-Based Estimation: Rotation Matrix Method

The dynamics-based aforementioned estimators are also compared with a kinematics-based estimation. In order to calculate the knee joint angle, the rotation matrix method involved using two frame transformations for each IMU. The knee joint angle was calculated by defining 2 unit vectors

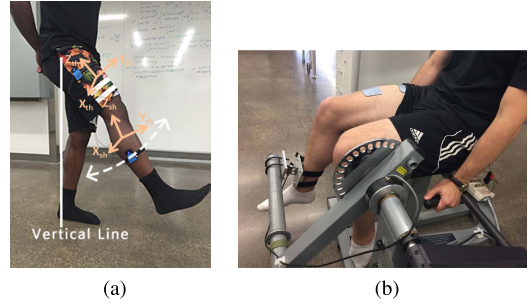


Fig. 3. (a) The hip flexion/extension rotations used to construct the IMU to body matrix. (b) The image above shows the experimental setup on an able-bodied participant.

along the longitudinal axes in the respective body coordinate systems and then transformed to a shared global frame to get the angle between the two vectors.

The equation below show how the angle was calculated from the body vectors expressed in the global frame.

$$\beta(t) = \cos^{-1} \left(\frac{\vec{v}_{ih}^g(t)}{\|\vec{v}_{ih}^g(t)\|} \cdot \frac{\vec{v}_{sh}^g(t)}{\|\vec{v}_{sh}^g(t)\|} \right), \quad (15)$$

where $\beta(t)$ is the knee joint angle at a given time, $\vec{v}_{ih}^g(t) \in \mathbb{R}^3$ and $\vec{v}_{sh}^g(t) \in \mathbb{R}^3$ represent the thigh and shank unit vectors along the longitudinal axes in the global frame of reference, respectively.

IV. EXPERIMENTS AND ESTIMATION RESULTS

The three estimators were experimentally compared on three able-bodied persons. The testing was performed after taking approval from the Institutional Review Board of the University of Pittsburgh. The objective of the estimation experiments was to estimate knee angle during FES of the quadriceps muscle. Three sets of experiments were conducted. The first set of the experiments was to find the IMU to body (alignment matrix) and IMU to global transformation matrices. The second set of experiments was performed to find the model parameters for the two dynamics-based estimators. The third set of experiments collected IMU data during FES of the quadriceps muscle while the participants sat on the leg extension machine. Finally, data collected from three sets of experiments was used, offline, by the 3 estimators to estimate the knee angle. The experimental set up is shown in Figs. (3a) and (3b).

A. Transformation Matrices

Either IMU to body (alignment matrix) or IMU to global transformation matrices, or both, were used to compute or estimate state in a reference frame as required by an estimation method. For example, the two dynamics-based estimation methods require system state to be in the body reference frame; thus, would need IMU to body transformation matrix. The rotation matrix method requires state to be in global reference frame.

1) *Alignment Matrix*: The alignment matrix, also called the IMU to body matrix (R_i^{th} and R_i^{sh}), was developed to transform measurements in the IMU frame of reference to the respective anatomical body coordinate system. In some

research studies, the IMU frame was assumed to coincide with the body frame [31]–[33]. This is not accurate because misalignment can occur due to the uneven body surface. Also, new methods are available to estimate the sensor to body alignment from arbitrary movements such as in [34]. For this paper the construction of this transformation matrix was derived from [35]–[37].

In order to define the body coordinate systems the subject was asked to stand still for 10 seconds and then perform three to five hip flexion/extension rotations. As Fig. 3a shows, two IMUs are placed firmly on the thigh and shank segments of the leg using electrical tape. The wireless communication between the IMUs and the wireless dongle was established in a program written in MATLAB 2015a (MathWorks Inc., USA) with a sample frequency of 100Hz. When the subject was standing still, the acceleration due to gravity was used to compute the Z axes in the body frame. Where the Z axes were considered to be parallel with gravity. The purpose for the hip flexion/extension rotations was to create a movement along each respective X axes in the body frames. Finally, the Y axes were computed by taking the cross product of the X and Z axes.

2) *IMU to Global Transformation Matrix*: For the rotation matrix estimation method, the IMU to global transformation (R_i^g) needs to be calculated in order to obtain the estimated knee joint angle. The procedure to create the IMU to global matrix was derived in [38]–[41]. A participant sat in the leg extension machine. During the stationary phase of the experiment, the initial rotation matrix is calculated using the accelerometer signals. Once the subject's leg is in motion the gyroscope signals are integrated to update the rotation matrix at each time step.

3) *Body to Global Matrix*: \vec{v}_{th}^g and \vec{v}_{sh}^g in Eq. (15) were computed as $\vec{v}_{th}^g(t) = R_{th}^g(t) \cdot \vec{v}^{th}$ and $\vec{v}_{sh}^g(t) = R_{sh}^g(t) \cdot \vec{v}^{sh}$, respectively, where $R_{th}^g \in \mathbb{R}^{3 \times 3}$ represents the thigh segment to global rotation matrix and was calculated as $R_{th}^g = R_{th}^i(t) \cdot R_{th}^i$. Similarly, $R_{sh}^g \in \mathbb{R}^{3 \times 3}$, which represents the shank segment to global rotation matrix, was calculated as $R_{sh}^g = R_{sh}^i(t) \cdot R_{sh}^i$.

B. Parameter Estimation

The parameters of the dynamic model in Eq. (6) are different for each individual, and these parameters need be determined before performing estimation. The experimental setup used to estimate the musculoskeletal parameters is shown in Fig. 3b, where the force from the participant can be measured by the load cell. An encoder was attached to the knee joint to record the true angle for error analysis later. Three able bodied persons participated in the experiment, where each leg was identified as a separate subject. All results of parameter estimation are shown in Table I. A more detailed description of the parameter estimation procedure can be found in [42]. The brief description of the parameter estimation procedure for each subject, collected during five different tests, is given below:

1. *Stimulation Ramp*: The subject was seated in the leg extension machine in an isometric configuration. The stimulation current amplitude was slowly increased

TABLE I
SUBJECT PARAMETERS OBTAINED FROM THE PARAMETER ESTIMATION PROCEDURE. L AND R REPRESENT THE SUBJECT'S LEFT AND RIGHT LEG, RESPECTIVELY

Parameter	Participant 1		Participant 2
	L	R	L
$\alpha[\frac{1}{kgm^2}]$	1.17	1.17	1.29
$\beta[\frac{1}{kgm^2}]$	40.90	40.90	40.28
ϕ_0 [rads]	0.40	8.34×10^{-11}	0.78
d_1 [Nm]	4.05	2.27	5.86
d_2 [Nms]	3.05	3.30	3.56
d_3 [Nm]	1.48×10^{-9}	3.96×10^{-8}	1.54×10^{-5}
d_4	14.10	11.20	8.70
d_5 [Nm]	8.90	15.30	3.05
d_6	-1.80	-1.77	-3.45
c_0 [Nm]	76.72	61.00	27.74
c_1 [Nm]	3.12	-0.57	295.32
c_2 [Nm]	-15.36	-8.47	-186.11
c_3	0.28	0.47	1.93×10^{-4}
θ_{eq} [rads]	0.13	0.08	0.19
T_a [Sec]	0.25	0.19	0.0044
I_t [mA]	33.90	38.60	33.50
I_s [mA]	60.40	68.20	66.60
RMSE[deg]	2.61	3.42	2.43
	Participant 2		Participant 3
	R	L	R
$\alpha[\frac{1}{kgm^2}]$	1.28	1.19	1.26
$\beta[\frac{1}{kgm^2}]$	40.28	47.34	39.43
ϕ_0 [rads]	2.22×10^{-14}	0.20	1.50
d_1 [Nm]	4.12	2.22×10^{-14}	4.41
d_2 [Nms]	2.54	3.14	2.60
d_3 [Nm]	2.38×10^{-5}	6.20	3.39×10^{-4}
d_4	8.34	0.84	6.70
d_5 [Nm]	5.41	0.04	0.16
d_6	-0.42	-30.22	-1.26×10^{-8}
c_0 [Nm]	-28.29	-17.88	5.63
c_1 [Nm]	402.07	299.41	159.39
c_2 [Nm]	-231.19	-183.75	-85.94
c_3	0.88	1.52	1.75
θ_{eq} [rads]	0.17	0.17	0.14
T_a [Sec]	1.00	0.72	0.18
I_t [mA]	38.80	38.20	32.9
I_s [mA]	64.90	68.10	63.2
RMSE[deg]	4.06	4.18	3.15

from I_{lower} to I_{upper} by increments of 3 mA with 2 second long pulses instead of a continuous current ramp to avoid muscle fatigue. 20mA and 80mA was chosen as the I_{lower} and I_{upper} respectively. These measurements were used to estimate the saturation and threshold current amplitudes (I_t and I_s in Eq. (5)). The threshold current amplitude, I_t , was defined as the first current amplitude that caused a significant muscle contraction (greater than 3 times the standard deviation of the load cell signal noise). The saturated current amplitude, I_s , was the last current amplitude applied in the stimulation ramp that caused the last significant increase in joint torque after the I_t was defined. The results of the stimulation ramp procedure for one participant can be seen in Fig. 4.

2. *Push/Pull*: These tests were performed by locking the subject's leg at different joint angles and measuring the output torque from the subject using the load cell. The results determined the passive stiffness parameters (d_1 , d_3 , d_4 , d_5 , and d_6), mass (m), and length (l_c) parameters. The parameters

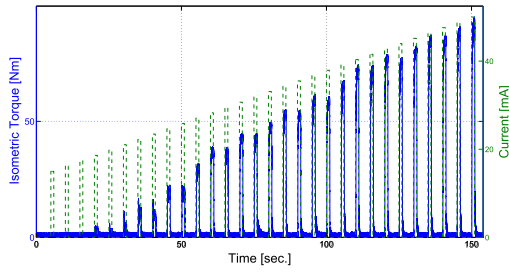


Fig. 4. Stimulation current ramp used to calculate the saturation and threshold current amplitudes (I_t and I_s).

were calculated by applying a nonlinear least-squares curve fitting algorithm to points plotted in the anatomical joint angle vs joint torque plane. The results of the procedure is shown in Fig. 5a.

3. Isometric Contractions: The torque-angle parameters (c_0 , c_1 , and c_2) were determined by performing multiple isometric contractions at seven different joint angles. Similar to the push/pull test, we used a nonlinear least-squares curve fitting algorithm to estimate the parameters. The curve fit is shown in Fig. 5b. All of the isometric contractions were performed at the saturation level, which means that they correspond to the maximum isometric joint torque at that joint angle. Therefore, it can be shown from (3) that normalizing these joint torques by their maximum values is equal to the activation (a_{ke}). Because it can be shown that the muscle activation is equal to the normalized joint torque during a maximum isometric contraction, the normalized load cell measurement would be approximately equal to muscle activation under this condition. The muscle activation time constant (T_a) was estimated by solving for the time constant of a first order response that best fit the response measured from the load cell, as shown in Fig. 5c.

4. Pendulum: In order to determine the damping and inertial parameters of the system (d_2 and α), a pendulum test was performed where the subject first held their leg at the full knee extension position and then released it to allow it to fall back to its neutral position. The encoder was used to measure the motion of leg, which included the oscillation and exponential decay of the position response. The pendulum response is a function of all of the parameters obtained in push and pull test except for d_2 . These previously determine parameters were used as constants in this test to determine d_2 and α . The measurement from encoder and the response from the best fit model were compared in order to calculate the parameters. Since the previous parameters are used for this test, some of the characteristics between measurement and the curve fit didn't match. This can be seen in Fig. 5d.

5. Sinusoidal Input: To find the torque-velocity relationship parameter, c_3 , a sinusoidal stimulation was applied to the quadriceps muscles of the subjects to produce knee extension/flexion. In order to keep the muscles in tension, a stimulation amplitude was applied so that the range of motion of the joint angle was between 10–70 degrees. The c_3 value was chosen by optimizing the value that would make the best fit. The sinusoidal response is shown in Fig. 6.

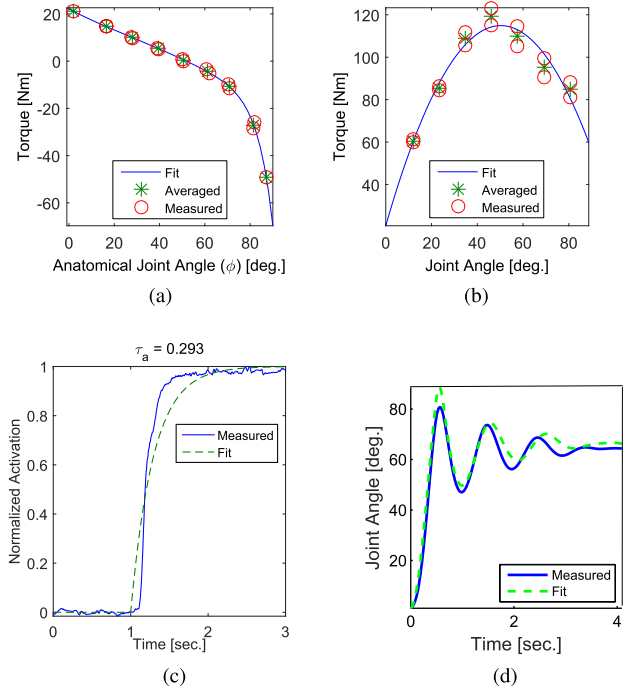


Fig. 5. (a) (b) The push/pull test used to determine the passive stiffness (d_1 , d_3 , d_4 , d_5 , and d_6) and mass parameters (m and I_c). (c) Isometric contractions test that determined the torque-angle (c_0 , c_1 , and c_2), activation time constant (T_a) and muscle activation (a_{ke}) parameters. (d) Pendulum test used to calculate the damping and inertial parameters (d_2 and α).

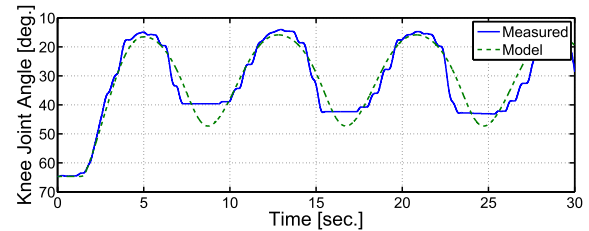


Fig. 6. The final sinusoidal input test used to determine the force-velocity parameter (c_3).

C. Estimation Experiments

Three able-bodied subjects sat in the leg extension machine while their quadriceps muscle was stimulated, as shown in Fig. 3b. Two IMUs (Yost Labs Inc., USA) are placed firmly on the thigh and shank segments of the leg using electrical tape. The wireless communication between the IMUs and the wireless dongle was established in a program written in Matlab 2015a with a sample frequency of 100Hz. To assess the performance of three estimators, the subject's motion was recorded using an rotary encoder (type: GHH100, produced by CALT) attached to the leg extension machine. The knee angle encoder data was acquired in a Matlab Simulink file with a sampling frequency of 1000Hz. Because the sampling frequencies between the two pieces of equipment did not match, the IMU data was interpolated by using Matlab's cubic spline data interpolation function. The FES (FNS-8 channel stimulator [CWE Inc., PA USA]) was applied to the quadriceps

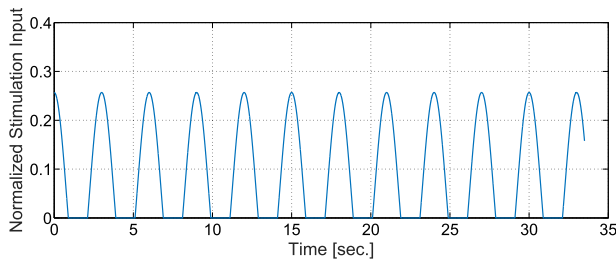


Fig. 7. The normalized stimulation input used for the leg extension test.

muscle to produce an involuntary motion, where the knee joint trajectory followed a sinusoidal curve. A typical normalized stimulation input, u , derived from Eq. (5), used to stimulate the muscle is shown in Fig. 7. Three 30 seconds experiments were performed on both legs of each subject. This created a total of 18 trials to analyze each estimator. Due to dropped data points between the IMUs some of the trials were discarded so only 17 trials are shown for EKF and SDC estimators and 15 trials are shown for the rotation matrix method. In the next subsection, the results of the three estimation methods (SDC, EKF and RMX), where estimation procedure was done offline, are presented.

D. Results

For the SDC estimator, ρ_i in (9) were chosen so that the root mean square error (RMSE) between the encoder and the estimated knee angle was minimized. An optimization method, using the `fmincon` function in MATLAB was used to find the optimal ρ_i . In order to apply the SDC estimator in a real application, the ρ_i needs to be tuned online. Methods similar to that described in [43] can be used in future studies to set ρ_i . Fig. 8(a) shows a typical comparison between each estimator for the left leg of person 2 trial 3. The results show that each estimator displayed the overall characteristics of the knee joint angle as it transitions from knee flexion to extension but the majority of the error occurred at the upper and lower peaks of the curves. The SDC estimator and EKF method compensate for most of the drift from the IMUs during upper and lower peaks compared to the rotation matrix method. Fig. 8(b) and (c) shows the other two state variables, x_2 and x_3 , over the time of the test.

The SDC estimator and EKF only used measurements from IMU on shank, while the rotation matrix used measurements from both IMU sensors. Results of 2 trials of rotation matrix were unavailable because the IMU on thigh dropped almost half of the data points during the experiment. Also, the last trial for participant 3 for the right leg was discarded due to possible cross talk between the IMU sensors. Table II shows all RMSEs of the estimation results of these three methods.

The Shapiro Wilk test was used to determine if the RMSE data were normal data sets. The test showed that the RMSE data sets are not normal distributions. Therefore, a Wilcoxon signed rank test with a 95% confidence level was used to determine if there was a statistically significant difference between the RMSEs of the 3 estimators. As shown in Fig. 9, based on the results of the Wilcoxon signed rank test, there

TABLE II
COMPARISON OF THE RMSEs (DEGREE) OF THE SDC-ESTIMATOR, EXTENDED KALMAN FILTER (EKF) AND ROTATION MATRIX (RMX). NA (NOT AVAILABLE) TRIALS WERE NOT INCLUDED IN THE AVERAGE

		RMSE [deg.]			
		Trial	SDC	EKF	RMX
Participant 1	L	1	1.71	2.46	3.21
		2	1.42	2.17	5.48
		3	2.02	2.77	3.88
		AVG	1.72	2.47	4.19
	R	1	2.37	2.61	0.81
		2	3.04	3.01	NA
		3	1.75	2.36	NA
AVG	2.39	2.66	0.81		
Participant 2	L	1	3.06	3.30	2.07
		2	1.06	1.61	1.18
		3	0.87	1.29	1.32
		AVG	1.66	2.07	1.52
	R	1	3.16	2.23	4.09
		2	3.39	4.16	6.69
		3	3.40	3.73	2.83
AVG	3.32	3.37	4.54		
Participant 3	L	1	3.42	11.87	1.68
		2	3.63	13.80	1.51
		3	6.51	7.91	1.89
		AVG	4.52	11.19	1.69
	R	1	2.40	6.36	2.40
		2	2.66	3.57	3.83
		3	NA	NA	NA
AVG	2.53	4.97	3.12		

exists a statistically significant difference between result of the SDC estimator and EKF.¹ While no statistically significant differences were found between the SDC estimator and rotation matrix and EKF methods and rotation matrix method.²

V. DISCUSSION

High performance closed loop control of FES requires accurate limb angle feedback. The feedback is usually obtained from optical encoders that are attached to limbs through exoskeletal rigid mechanical attachments. To enable wearability of FES devices, an IMU would be a better option than using an angular encoder, which would require an exoskeletal set-up. However, IMUs are susceptible to drift and noise, leading to inaccurate limb angle estimates. In this paper, a new class of nonlinear estimators called the SDC estimator was used to estimate the knee joint motion during FES. The use of the SDC estimator overcomes limitations of Jacobian linearization (e.g., in EKF) by considering an alternate formulation called extended linearization. The new single joint angle estimation method provides a preliminary evidence of better performance vis-à-vis EKF and kinematics-based rotation matrix method. The experimental results showed that

¹The critical test statistic value for a sample size of 17 and a significance level is 0.05, and the results of the Wilcoxon test was determined to be 0.0032. Since the calculated test statistic is smaller than the significance level, it was concluded that there is statistical difference between the two data sets.

²The critical test statistic value for a sample size of 15 and a significance level is 0.05, and the results of the Wilcoxon test was determined to be 0.8729 and 0.3421 for the comparison between the SDC and rotation matrix and the EKF and the rotation matrix respectively. Since the calculated test statistic is larger than the significance level, it was concluded that there is no statistical difference between the two data sets.

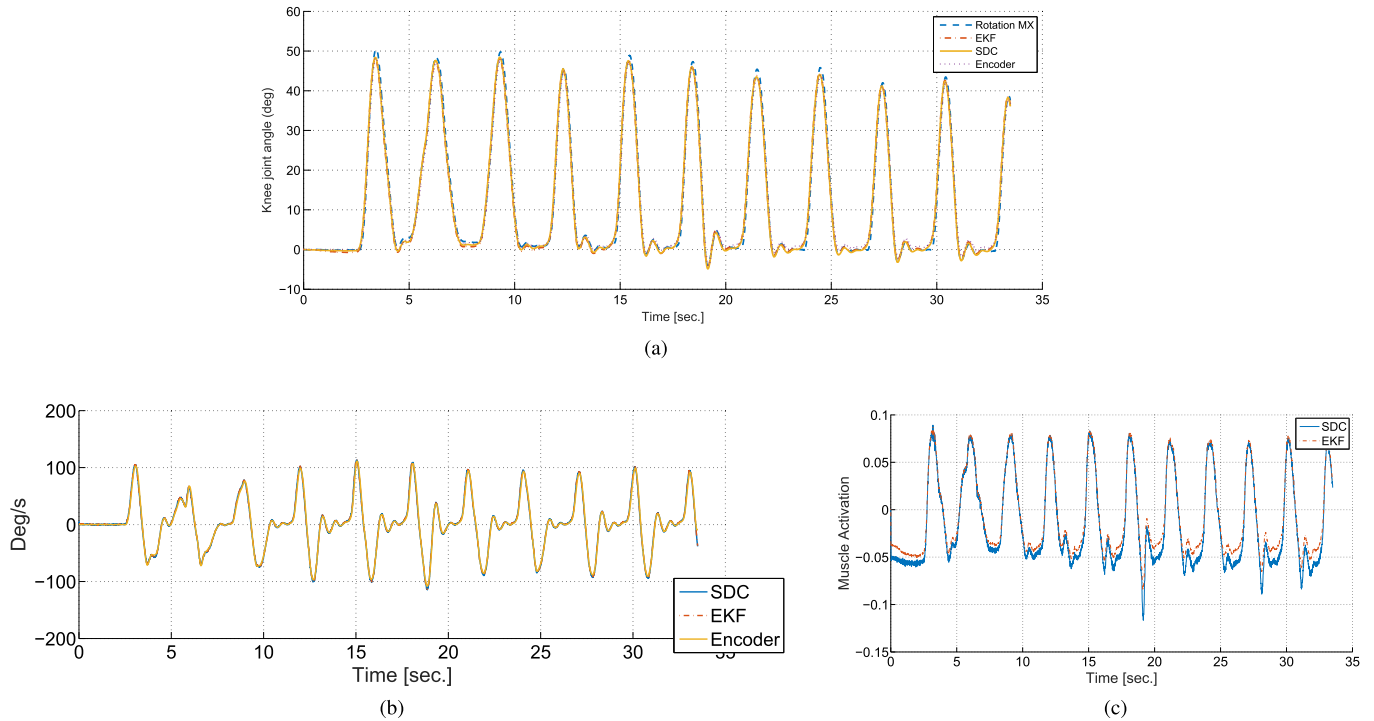


Fig. 8. (a) Knee joint angle estimation comparison of the left leg of person 2-trial 3. (b) Plot comparing \hat{x}_2 of each estimator to the filtered time derivative of the encoder signal. (c) The plot of \hat{x}_3 of each estimator over the testing period.

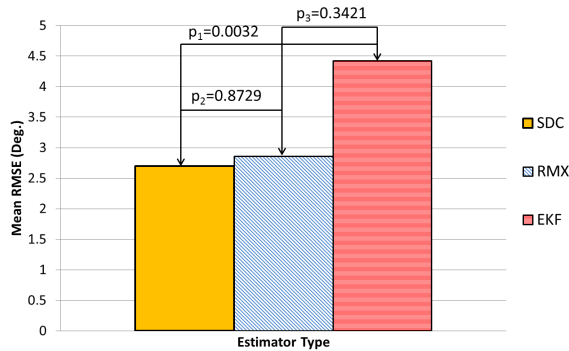


Fig. 9. Result of Wilcoxon signed rank test.

the SDC estimator, the rotation matrix method, and the EKF method had root mean square errors of 2.70° , 2.86° , and 4.42° , respectively.

Unlike the EKF method, the method employs SDC parameterization, which is a form of an extended linearization, to compute optimal error covariance and gain of the estimators. In the Appendix, we show the derived SDC parameterization used for the estimator. The SDC estimator performed well compared to EKF fusion orientation tracking algorithms described in [18] and [19], where an additional magnetic sensor was implemented, but a dynamic model was absent. Their results showed that the lowest RMSE was 2.3° , which occurred during 10 trials of an upper arm abduction movement. Even though the magnetic sensor can be used to counter the gyroscope drift, the dynamic model-based estimator may provide a better estimate and a more reliable estimator for ambulatory tracking. Especially when the use of magnetic

sensor is hard to predict when the magnetic disturbance is present.

The preliminary results show the new estimator's advantage over the EKF method but a slight advantage over the rotation matrix method. However, the information from the dynamic model allows the SDC method to use only one IMU to measure the knee angle compared to the rotation matrix method that used 2 IMUs to estimate the knee angle. Another main weakness of the rotation matrix method is that it does not account for the gyroscope drift after subtracting the initial bias. This was not highlighted due to the test only running for 30 seconds, which displays an insignificant amount of drift. If the SDC estimator and the rotation matrix were used in a real world application, the SDC will show a superior performance since it compensates for the gyroscope drift online.

Nonetheless, there are limitations of the new method such as an effort in model identification, precise knowledge of muscular inputs, and tuning of parameters. The ρ_i parameters were tuned offline with the angular encoder as a true reference signal. In order to extend the SDC estimator for real time applications, i.e. without the encoder, methods in [25] and [29] can be used in future studies. Errors during parameter estimation procedure may lead to error in the estimation. So accuracy of model identification procedure is critical. In some FES applications, the model may be already available (e.g., see model-based control design methods [44], [45]). Then the model identification procedure can be bypassed and the available model can be used in the estimator design. To obtain the musculoskeletal parameters during home use by persons with stroke or SCI, equipment and parameter estimation methods similar to that described in [43] can be used. Volitional

inputs can be provided to the SDC estimator as well to include volitional ability of a user. Then the SDC estimator can be extended to correct gait of persons with stroke, who have residual volitional drive. To predict residual volitional drive by a person with stroke, measurements of the volitional motion and contact forces in the leg can be captured through electromyography and force sensitive resistors, respectively.

Finally, we intend to implement the SDC estimator in FES applications that include drop-foot correction and walking restoration. Our current work focuses only on estimation design for a single joint. The results in the paper are preliminary and the estimator's performance during gait still remains to be tested. Also, our future goal is to combine the SDC estimator with a control design for FES (e.g., in [7], [8], [46], and [47]) that uses IMUs for feedback. Combining SDC estimator with an FES controller would require proving convergence of a nonlinear estimator and controller stability at the same time, which is an open research problem.

VI. CONCLUSION

A new method of estimation called the SDC estimator was introduced. The knee joint motion during FES of the quadriceps muscle was measured by using IMUs. The knee dynamics was used instead of a kinematics-based measurement model. The statistical analysis results show that the SDC estimator's performance is statistically significantly different from the EKF method, which uses a linearized model. Future work, will go into integrating the SDC estimator with a closed-loop FES controller that uses IMU sensors to measure limb state.

APPENDIX

SDC Parameterizations: The SDC parameterizations, given below, were used for the SDC estimator as described in Section III-A. These matrices were designed such that each parameterization, $A_i(x)$, captures the system dynamics, i.e., $A_i(x)x = f(x, u)$.

$$A_1 = \begin{bmatrix} 0 & 1 & 0 \\ A_1^{21} & A_1^{22} & A_1^{23} \\ 0 & 0 & -\frac{1}{T_a} \end{bmatrix}$$

$$A_1^{21} = \frac{-\beta \sin(x_1)}{x_1} - [d_1 + (c_2(\pi - x_1) + c_1)x_3 + \varepsilon_1 - \varepsilon_2]\alpha$$

$$A_1^{22} = \alpha[-d_2 - c_3x_3((c_2\frac{\pi^2}{4} + c_1\frac{\pi}{2} + c_0) + x_1(c_2(\pi - x_1) + c_1))]$$

$$A_1^{23} = \alpha[c_2\frac{\pi^2}{4} + c_1\frac{\pi}{2} + c_0]$$

$$A_2 = \begin{bmatrix} 0 & 1 & 0 \\ A_2^{21} & A_2^{22} & A_2^{23} \\ 0 & 0 & -\frac{1}{T_a} \end{bmatrix}$$

$$A_2^{21} = \frac{-\beta \sin(x_1)}{x_1} - [d_1 + (c_2(\pi - x_1) + c_1)x_3 + \varepsilon_1 - \varepsilon_2]\alpha$$

$$A_2^{22} = \alpha[-d_2 - c_3x_3(c_2\frac{\pi^2}{4} + c_1\frac{\pi}{2} + c_0)]$$

$$A_2^{23} = \alpha[c_2\frac{\pi^2}{4} + c_1\frac{\pi}{2} + c_0 + c_3x_1x_2(c_2(\pi - x_1) + c_1)]$$

$$A_3 = \begin{bmatrix} 0 & 1 & 0 \\ A_3^{21} & A_3^{22} & A_3^{23} \\ 0 & 0 & -\frac{1}{T_a} \end{bmatrix}$$

$$A_3^{21} = \frac{-\beta \sin(x_1)}{x_1} - \alpha[d_1 + (1 - c_3x_2)(c_2(\pi - x_1) + c_1)x_3 + \varepsilon_1 - \varepsilon_2]$$

$$A_3^{22} = \alpha[-d_2 - c_3x_3(c_2\frac{\pi^2}{4} + c_1\frac{\pi}{2} + c_0)]$$

$$A_3^{23} = \alpha[c_2\frac{\pi^2}{4} + c_1\frac{\pi}{2} + c_0]$$

$$A_4 = \begin{bmatrix} 0 & 1 & 0 \\ A_4^{21} & A_4^{22} & A_4^{23} \\ 0 & 0 & -\frac{1}{T_a} \end{bmatrix}$$

$$A_4^{21} = \frac{-\beta \sin(x_1)}{x_1} - \alpha d_1 + \varepsilon_1 - \varepsilon_2$$

$$A_4^{22} = \alpha[-d_2 + c_3x_1x_3(c_2(\pi - x_1) + c_1)]$$

$$A_4^{23} = \alpha[-(c_2(\pi - x_1) + c_1)x_1 - c_3x_2(c_2\frac{\pi^2}{4} + c_1\frac{\pi}{2} + c_0) + c_2\frac{\pi^2}{4} + c_1\frac{\pi}{2} + c_0]$$

In the above terms, ε_1 and ε_2 are defined as $\varepsilon_1 = d_3e^{d_4\frac{\pi}{2}}\frac{(e^{-d_4x_1}-1)}{x_1}$, $\varepsilon_2 = d_5e^{d_6\frac{\pi}{2}}\frac{(e^{-d_6x_1}-1)}{x_1}$.

Covariance Matrices: The following covariances matrices were used for both the SDC and EKF estimators. $Q =$

$$\begin{bmatrix} 0 & 0 & 0 \\ 0 & 1.5084 & 0 \\ 0 & 0 & 1.5084 \end{bmatrix}, S = \begin{bmatrix} 0.009 & 0 \\ 0 & 20 \end{bmatrix}.$$

REFERENCES

- [1] J. P. Giuffrida and P. E. Crago, "Functional restoration of elbow extension after spinal-cord injury using a neural network-based synergistic FES controller," *IEEE Trans. Neural Syst. Rehabil. Eng.*, vol. 13, no. 2, pp. 147–152, Jun. 2005.
- [2] M. Popovic, D. Popovic, and T. Keller, "Neuroprostheses for grasping," *Neurol. Res.*, vol. 24, no. 5, pp. 443–452, 2002.
- [3] T. Bajd, A. Kralj, R. Turk, H. Benko, and J. Šega, "The use of a four-channel electrical stimulator as an ambulatory aid for paraplegic patients," *Phys. Therapy*, vol. 63, no. 7, pp. 1116–1120, 1983.
- [4] R. B. Stein *et al.*, "Long-term therapeutic and orthotic effects of a foot drop stimulator on walking performance in progressive and nonprogressive neurological disorders," *Neurorehabil. Neural Repair*, vol. 24, no. 2, pp. 152–167, Feb. 2010. [Online]. Available: <http://nnr.sagepub.com/content/24/2/152>
- [5] T. C. Bulea, R. Kobetic, M. L. Audu, J. R. Schnellenberger, and R. J. Triolo, "Finite state control of a variable impedance hybrid neuroprosthesis for locomotion after paralysis," *IEEE Trans. Neural Syst. Rehabil. Eng.*, vol. 21, no. 1, pp. 141–151, Jan. 2013.
- [6] L. Lovse, J. Bobet, F. D. Roy, R. Rolf, V. K. Mushahwar, and R. B. Stein, "External sensors for detecting the activation and deactivation times of the major muscles used in walking," *IEEE Trans. Neural Syst. Rehabil. Eng.*, vol. 20, no. 4, pp. 488–498, Jul. 2012. [Online]. Available: <http://www.ncbi.nlm.nih.gov/pubmed/22717527>
- [7] C. T. Freeman, E. Rogers, A.-M. Hughes, J. H. Burridge, and K. L. Meadmore, "Iterative learning control in health care: Electrical stimulation and robotic-assisted upper-limb stroke rehabilitation," *IEEE Control Syst.*, vol. 32, no. 1, pp. 18–43, Feb. 2012.
- [8] N. Sharma, K. Stegath, C. M. Gregory, and W. E. Dixon, "Nonlinear neuromuscular electrical stimulation tracking control of a human limb," *IEEE Trans. Neural Syst. Rehabil. Eng.*, vol. 17, no. 6, pp. 576–584, Dec. 2009.
- [9] R. E. Mayagoitia, A. V. Nene, and P. H. Veltink, "Accelerometer and rate gyroscope measurement of kinematics: An inexpensive alternative to optical motion analysis systems," *J. Biomech.*, vol. 35, no. 4, pp. 537–542, Apr. 2002. [Online]. Available: <http://www.sciencedirect.com/science/article/pii/S0021929001002317>

- [10] I. P. I. Pappas, M. R. Popovic, T. Keller, V. Dietz, and M. Morari, "A reliable gait phase detection system," *IEEE Trans. Neural Syst. Rehabil. Eng.*, vol. 9, no. 2, pp. 113–125, Jul. 2001. [Online]. Available: <http://www.ncbi.nlm.nih.gov/pubmed/11474964>
- [11] R. A. Hyde, L. P. Ketteringham, S. A. Neild, and R. J. S. Jones, "Estimation of upper-limb orientation based on accelerometer and gyroscope measurements," *IEEE Trans. Biomed. Eng.*, vol. 55, no. 2, pp. 746–754, Feb. 2008.
- [12] C. C. Monaghan, W. J. B. M. van Riel, and P. H. Veltink, "Control of triceps surae stimulation based on shank orientation using a uniaxial gyroscope during gait," *Med. Biol. Eng. Comput.*, vol. 47, no. 11, pp. 1181–1188, Nov. 2009.
- [13] D. Kotiadis, H. J. Hermens, and P. H. Veltink, "Inertial Gait Phase Detection for control of a drop foot stimulator: Inertial sensing for Gait Phase Detection," *Med. Eng. Phys.*, vol. 32, no. 4, pp. 287–297, May 2010.
- [14] R. Williamson and B. J. Andrews, "Detecting absolute human knee angle and angular velocity using accelerometers and rate gyroscopes," *Med. Biol. Eng. Comput.*, vol. 39, no. 3, pp. 294–302, 2001.
- [15] Y. Zhang, K. Chen, J. Yi, T. Liu, and Q. Pan, "Whole-body pose estimation in human bicycle riding using a small set of wearable sensors," *IEEE/ASME Trans. Mechatronics*, vol. 21, no. 1, pp. 163–174, Feb. 2016.
- [16] Y. Zhang, K. Chen, and J. Yi, "Rider trunk and bicycle pose estimation with fusion of force/inertial sensors," *IEEE Trans. Biomed. Eng.*, vol. 60, no. 9, pp. 2541–2551, Sep. 2013.
- [17] Z.-Q. Zhang, W.-C. Wong, and J.-K. Wu, "Ubiquitous human upper-limb motion estimation using wearable sensors," *IEEE Trans. Inf. Technol. Biomed.*, vol. 15, no. 4, pp. 513–521, Jul. 2011.
- [18] H. M. Schepers, D. Roetenberg, and P. H. Veltink, "Ambulatory human motion tracking by fusion of inertial and magnetic sensing with adaptive actuation," *Med. Biol. Eng. Comput.*, vol. 48, pp. 27–37, Jan. 2010.
- [19] D. Roetenberg, P. J. Slycke, and P. H. Veltink, "Ambulatory position and orientation tracking fusing magnetic and inertial sensing," *IEEE Trans. Biomed. Eng.*, vol. 54, no. 5, pp. 883–890, May 2007.
- [20] C. Wong, Z.-Q. Zhang, B. Lo, and G.-Z. Yang, "Wearable sensing for solid biomechanics: A review," *IEEE Sensors J.*, vol. 15, no. 5, pp. 2747–2760, May 2015.
- [21] H. J. Luinge and P. H. Veltink, "Measuring orientation of human body segments using miniature gyroscopes and accelerometers," *Med. Biol. Eng. Comput.*, vol. 43, no. 2, pp. 273–282, Mar. 2005.
- [22] H. Fourati, N. Manamanni, L. Afilal, and Y. Handrich, "Position estimation approach by complementary filter-aided IMU for indoor environment," in *Proc. Eur. Control Conf. (ECC)*, Jul. 2013, pp. 4208–4213.
- [23] F. Widjaja, C. Y. Shee, W. L. Au, P. Poignet, and W. T. Ang, "An extended Kalman filtering of accelerometer and surface electromyography data for attenuation of pathological tremor," in *Proc. 2nd IEEE RAS EMBS Int. Conf. Biomed. Robot. Biomech.*, Oct. 2008, pp. 193–198.
- [24] T. Bennett, R. Jafari, and N. Gans, "An extended Kalman filter to estimate human gait parameters and walking distance," in *Proc. ACC*, 2013, pp. 752–757.
- [25] A. Dani and N. Sharma, "A discrete-time nonlinear estimator for an orthosis-aided gait," in *Proc. ASME Dyn. Syst. Control Conf.*, San Antonio, TX, USA, Oct. 2014, p. V001T04A003.
- [26] N. Sharma and A. Dani, "Nonlinear estimation of gait kinematics during functional electrical stimulation and orthosis-based walking," in *Proc. IEEE ACC*, Jun. 2014, pp. 4778–4783.
- [27] N. Sharma, V. Mushahwar, and R. Stein, "Dynamic optimization of FES and orthosis-based walking using simple models," *IEEE Trans. Neural Syst. Rehabil. Eng.*, vol. 22, no. 1, pp. 114–126, Jan. 2014.
- [28] A. P. Dani, S.-J. Chung, and S. Hutchinson, "Observer design for stochastic nonlinear systems using contraction analysis," in *Proc. 51st IEEE CDC*, Dec. 2012, pp. 6028–6035.
- [29] A. P. Dani, S.-J. Chung, and S. Hutchinson, "Observer design for stochastic nonlinear systems via contraction-based incremental stability," *IEEE Trans. Autom. Control*, vol. 60, no. 3, pp. 700–714, Mar. 2015.
- [30] M. Zhang, "Multi-sensor inertial measurement system for analysis of sports motion," Ph.D. dissertation, Swanson School Eng., Univ. Pittsburgh, Pittsburgh, PA, USA, 2014.
- [31] K. Liu, T. Liu, K. Shibata, Y. Inoue, and R. Zheng, "Novel approach to ambulatory assessment of human segmental orientation on a wearable sensor system," *J. Biomech.*, vol. 42, no. 16, pp. 2747–2752, 2009.
- [32] K. Sagawa, S. Abo, T. Tsukamoto, and I. Kondo, "Forearm trajectory measurement during pitching motion using an elbow-mounted sensor," *J. Adv. Mech. Des., Syst., Manuf.*, vol. 3, no. 4, pp. 299–311, 2009.
- [33] M. El-Gohary and J. McNames, "Shoulder and elbow joint angle tracking with inertial sensors," *IEEE Trans. Biomed. Eng.*, vol. 59, no. 9, pp. 2635–2641, Sep. 2012.
- [34] T. Seel, J. Raisch, and T. Schauer, "IMU-based joint angle measurement for gait analysis," *Sensors*, vol. 14, no. 4, pp. 6891–6909, 2014.
- [35] J. Favre, R. Aissaoui, B. M. Jolles, J. A. de Guise, and K. Aminian, "Functional calibration procedure for 3D knee joint angle description using inertial sensors," *J. Biomech.*, vol. 42, no. 14, pp. 2330–2335, 2009.
- [36] H. J. Luinge, P. H. Veltink, and C. T. M. Baten, "Ambulatory measurement of arm orientation," *J. Biomech.*, vol. 40, no. 1, pp. 78–85, Jan. 2007.
- [37] J. Favre, B. M. Jolles, R. Aissaoui, and K. Aminian, "Ambulatory measurement of 3D knee joint angle," *J. Biomech.*, vol. 41, no. 5, pp. 1029–1035, 2008.
- [38] A. M. Sabatini, "Quaternion-based extended Kalman filter for determining orientation by inertial and magnetic sensing," *IEEE Trans. Biomed. Eng.*, vol. 53, no. 7, pp. 1346–1356, Jul. 2006.
- [39] J. S. Wang, Y. L. Hsu, and J. N. Liu, "An inertial-measurement-unit-based pen with a trajectory reconstruction algorithm and its applications," *IEEE Trans. Ind. Electron.*, vol. 57, no. 10, pp. 3508–3521, Oct. 2010.
- [40] J. Diebel, "Representing attitude: Euler angles, unit quaternions, and rotation vectors," *Matrix*, vol. 58, nos. 15–16, pp. 1–35, 2006.
- [41] J. B. Kuipers, *Quaternions and Rotation Sequences*, vol. 66. Princeton, NJ, USA: Princeton Univ. Press 1999.
- [42] N. Kirsch, N. Alibeji, and N. Sharma, "Nonlinear model predictive control of functional electrical stimulation," *Control Eng. Pract.*, vol. 58, pp. 319–331, Jan. 2017.
- [43] M. Benoussaad, K. Mombaur, and C. Azevedo-Coste, "Nonlinear model predictive control of joint ankle by electrical stimulation for drop foot correction," in *Proc. IEEE/RSJ Int. Conf. Intell. Robots Syst. (IROS)*, Nov. 2013, pp. 983–989.
- [44] M. Ferrarin, F. Palazzo, R. Riener, and J. Quintern, "Model-based control of FES-induced single joint movements," *IEEE Trans. Neural Syst. Rehabil. Eng.*, vol. 9, no. 3, pp. 245–257, Sep. 2001.
- [45] R. Riener and T. Fuhr, "Patient-driven control of FES-supported standing up: A simulation study," *IEEE Trans. Rehabil. Eng.*, vol. 6, no. 2, pp. 113–124, Jun. 1998.
- [46] N. Sharma, C. M. Gregory, and W. E. Dixon, "Predictor-based compensation for electromechanical delay during neuromuscular electrical stimulation," *IEEE Trans. Neural Syst. Rehabil. Eng.*, vol. 19, no. 6, pp. 601–611, Dec. 2011.
- [47] N. Alibeji, N. Kirsch, S. Farrokhi, and N. Sharma, "Further results on predictor-based control of neuromuscular electrical stimulation," *IEEE Trans. Neural Syst. Rehabil. Eng.*, vol. 23, no. 6, pp. 1095–1105, Nov. 2015.

Authors' photographs and biographies not available at the time of publication.